

Tuning ferromagnetism in zinc oxide nanoparticles by chromium doping

Palvinder Kaur · S. K. Pandey · Sanjeev Kumar ·
N. S. Negi · C. L. Chen · S. M. Rao ·
M. K. Wu

Received: 26 November 2014 / Accepted: 17 December 2014 / Published online: 1 January 2015
© The Author(s) 2014. This article is published with open access at Springerlink.com

Abstract $Zn_{1-x}Cr_xO$ nanoparticles with $x = 0.0, 0.01, 0.03$ and 0.05 were synthesized by the sol–gel technique. Powder X-ray diffraction (XRD) studies reveal that chromium (Cr) incorporates into the ZnO crystal lattice without disturbing the parent hexagonal (wurtzite) structure. Transmission electron microscopy (TEM) measurements show that the average size of these nanoparticles is in the range 15–25 nm. Optical absorption studies show that the band gap of ZnO nanoparticles varies with Cr doping. Photoluminescence (PL) studies depict the presence of defects in Cr-doped nanoparticles. Undoped ZnO exhibits diamagnetic behavior while Cr-doped ZnO samples exhibit weak ferromagnetism to anti-ferromagnetism depending on the Cr content.

Keywords ZnO · Ferromagnetism · Nanoparticles · Sol–gel

Introduction

The marriage of semiconductors and magnetism has led to the next generation of magnetic semiconductors, where it is not the electron charge but the electron spin that carries information (Sato and Katayama-Yoshida 2000). Replacement of cations in a non-magnetic semiconductor by small doping of magnetic transition metal ions resulted in new class of semiconductors known as diluted magnetic semiconductors (DMSs) (Sato and Katayama-Yoshida 2000; Katayama-Yoshida and Sato 2003; Wolf et al. 2001; Dietl 2002). These materials show magnetic properties, from para-magnetism to ferromagnetism and play a vital role in the field of spin transport electronics (Spintronics). Initially, II–VI semiconductor (CdTe and ZnSe)-based magnetic semiconductors were studied. On doping with Mn, these could be used as optical isolator (Onodera et al. 1994) and giant magnetoresistance (GMR) devices (Baibich et al. 1988; Barnas et al. 1990). In such DMS, the ferromagnetism could be achieved at low Curie temperature (T_c) making these materials less attractive for industrial applications. Ohno (1998) proposed that the doping of III–V semiconductors exhibits ferromagnetism at high T_c (beyond room temperature), because of strong p – d exchange interactions intermediated by the mobile holes. To get rid of this difficulty, oxide-based semiconductors were investigated speedily. Deep-level intrinsic defects and complexes may be the origin of the room temperature ferromagnetism observed in oxide-based semiconductors (Ohno 1998).

The first principle band calculation by Sato and Katayama (2002) showed that the ZnO doped with V, Cr, Fe, Co and Ni can be ferromagnetic. Their theoretical calculations proved that the magnetic states are controllable by changing the carrier density. ZnO nanostructures act as an

P. Kaur · S. K. Pandey · S. M. Rao
Department of Physics, Punjabi University, Patiala 147002, India

S. K. Pandey
Gandhi Memorial National College, Ambala Cantt 133001, India

S. Kumar (✉)
Applied Science Department, PEC University of Technology,
Chandigarh 160012, India
e-mail: sanjeevace_phy@yahoo.co.in

N. S. Negi
Department of Physics, Himachal Pradesh University,
Shimla 171005, India

C. L. Chen · S. M. Rao · M. K. Wu
Institute of Physics, Academia Sinica, Taipei 11529, Taiwan

excellent semiconductor host for the transition metal dopant atoms because of the exchange interactions between the spin of the dopant atoms and the carriers in the ZnO matrix and generate a ferromagnetic order in the entire lattice at room temperature (Furdyna 1988). More research in the field of DMS resulted in various transition metal-doped ZnO which exhibited room temperature ferromagnetism (RTFM) such as Cr (Duan et al. 2010; Li and Hu 2011; Babu et al. 2014), Co, Fe, Ni, Mn, V and Ru (Gandhi et al. 2014; Kataoka et al. 2010a, b; Pazhanivelu et al. 2014; Omria et al. 2013; Olive-Mendez et al. 2014; Kumar et al. 2014). In the present investigation, we have chosen Cr as dopant because (1) Cr^{3+} is an important transition metal element having ionic radius smaller than Zn^{2+} and substitutes Zn^{2+} in the lattice, (2) theoretical research also supports the prospect of producing ferromagnetism in chromium-based DMSs (Sato and Katayama 2002) and (3) few reports are available on room-temperature ferromagnetism in Cr-doped ZnO.

Experimental details

In the present investigations, Cr-doped ZnO nanoparticles were synthesized by sol–gel technique. In this study, zinc acetate dihydrate, chromium acetate, 2-methoxyethanol and monoethanolamine (MEA) were used as the starting materials, solvent and stabilizer, respectively. Zinc acetate dihydrate and chromium acetate were first dissolved in 2-methoxyethanol. The molar ratio of MEA to zinc acetate dihydrate was maintained at 1. The resulting mixture was stirred at 60 °C for 2 h. When the mixture was stirred, MEA was added drop by drop. Finally, a clear and transparent homogeneous solution was formed. The total concentration of solution was kept at 0.5 mol/L and the concentration of chromium 1, 3 and 5 mol% with respect to zinc. The sol was aged for 24 h at room temperature. Then sol was dried in a furnace at 400 °C for 1 h. Then, the dry samples were crushed in pestle mortar to get the fine powder. Then, the fine powder was annealed at 500 °C for 1 h.

The X-ray diffraction (XRD) studies of $\text{Zn}_{1-x}\text{Cr}_x\text{O}$ nanoparticles were investigated using “Panalytical Xpert Diffractometer”. The particle size determination and structure confirmations were made using a FEI G² high-resolution transmission electron microscopy (HR-TEM) coupled with an energy-dispersive X-ray analysis (EDX) accessory. Optical absorption measurements were made using a standard UV–Vis spectrophotometer by dispersing the powders in water. Magnetic measurements were made using a Vibrating Sample Magnetometer (VSM) operated from –5 to +5 kOe at room temperature.

Results and discussion

The XRD patterns of the $\text{Zn}_{1-x}\text{Cr}_x\text{O}$ nanoparticles are shown in Fig. 1. On comparing with standard sample as per JCPDS card (card no: JCPDS-36-1451), all the diffraction peaks of the prepared nanoparticles can be well indexed to the wurtzite (hexagonal phase) of ZnO ($a = b = 3.25 \text{ \AA}$, $c = 5.20 \text{ \AA}$). It reveals that the peaks correspond to diffraction at (100), (002), (101), (102), (110), (103), (200), (112) and (201) lattice planes. It is seen from the XRD patterns as shown in Fig. 1 that the peaks of ZnO shift towards higher angles with increasing Cr concentration in $\text{Zn}_{1-x}\text{Cr}_x\text{O}$ samples indicating a decrease in the lattice parameters. This clearly depicts the replacement of Zn^{2+} (0.74 Å) by Cr^{3+} (0.63 Å). The shift to higher 2θ is lesser in the $x = 0.05$ sample probably due to the formation of secondary phases. Peaks related to weak secondary phase (ZnCr_2O_4 , marked with asterisk) are observed at $x = 0.05$. These two observations are consistent with the reports of Duan et al. (2010). The mean crystallite size was estimated using Scherrer’s formula $D = k\lambda/\beta\cos\theta$, where D is the mean grain size, k is a geometric factor, $k = 0.89$, $\lambda = 0.154056 \text{ nm}$ is the X-ray wavelength used, β is the FWHM of diffraction peak and θ is the diffraction angle. The estimated size is around 22 nm in corroboration with TEM results.

TEM image of Cr-doped ZnO nanoparticles is shown in Fig. 2. Average size observed from TEM image is around 25 nm, which is in agreement with size calculated from XRD data. By observing the lattice fringes from HRTEM of Cr-doped ZnO nanoparticles (Fig. 3), the interplanar distance is found to be 0.26 nm (2.6 nm is along 10

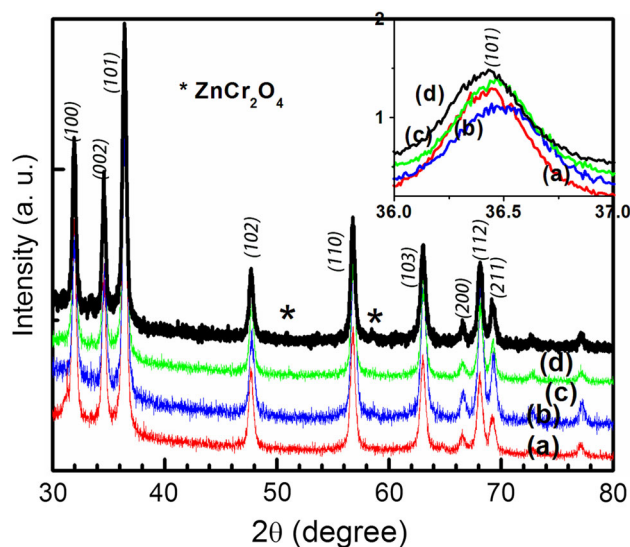


Fig. 1 XRD pattern of $\text{Zn}_{1-x}\text{Cr}_x\text{O}$ ($a-d$) $x = 0, 0.01, 0.03$ and 0.05 respectively. Inset shows an expanded view of doping induced peak shift in the prepared $\text{Zn}_{1-x}\text{Cr}_x\text{O}$ nanoparticles

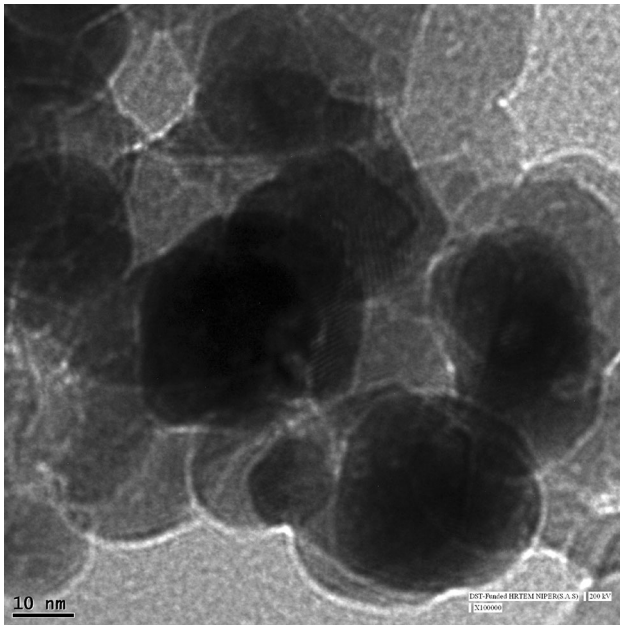


Fig. 2 TEM image of Cr-doped ZnO nanoparticles

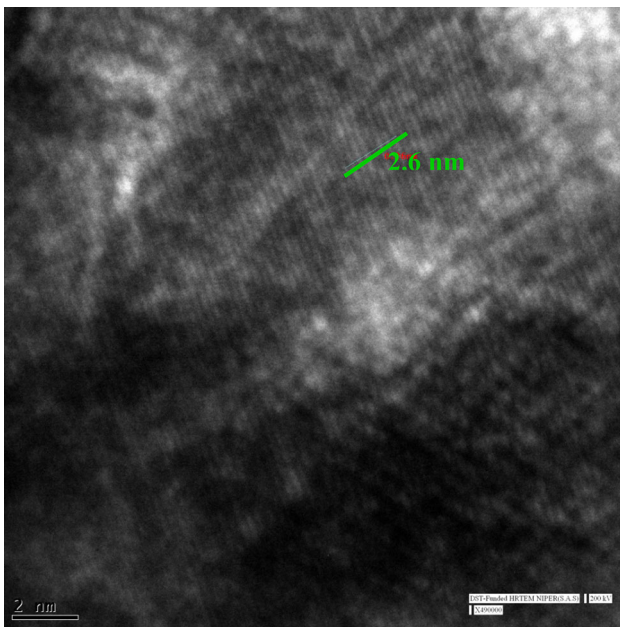


Fig. 3 HRTEM image of Cr-doped ZnO nanoparticle depicting lattice fringes and interplanar spacing

interplanar spacings), matching the (002) planes of the wurtzite ZnO, which is in agreement with calculations from XRD data. The local chemical compositions of the samples were characterized by energy-dispersive X-ray spectroscopy (EDS). Figure 4 shows the existence of zinc, oxygen and chromium in ZnO nanoparticles. EDS was performed at several different locations in the same nanoparticle, resulting in the identification of similar chemical

compositions, which suggests a fairly uniform distribution of the dopant ions.

The optical absorption spectra recorded for the above samples by suspending them in water after long time sonication are shown in Fig. 5. A peak is observed at 365 nm which shifts to a lower value as x is increased. This shift is reduced in the $x = 0.05$ sample in corroboration with the XRD results discussed above. To calculate the optical band gap (E_g) employing Tauc's plot, the variation of the absorption coefficient with photon energy is studied using the relation:

$$\alpha(h\nu) = A(h\nu - E_g)^{1/2}$$

where E_g is the optical band gap and A is a constant. Figure 6 shows the plot of $(\alpha h\nu)^2$ versus $(h\nu)$ for the pure and doped ZnO samples.

Band gap values are estimated by extrapolating the linear portions of the plots onto the energy axis and these analyses show an apparent increase in E_g from 3.06 to 3.11 eV with an increase of Cr content from $x = 0.00$ to 0.03. Semiconductor particles having size greater than ‘‘Bohr radius’’ are coming under weak confinement regime. Size is very important even in weak confinement regime (Pandiyarajan and Karthikeyan 2012). TEM micrographs (Fig. 2) depict that the prepared particles are lying in this regime. In the present study, Cr plays a decisive role in tuning the band gap. Band gap of the particle will increase with decrease in the particle size as per the following relation (Dijken et al. 2000):

$$E_n = E_g - E_{\text{exc}} + (\hbar^2 \pi^2 n^2 / 2MR^2)$$

where $M = m_e + m_h$ is the total mass of the e–h pair, ‘ R ’ is the radius of the nanoparticle, ‘ E_g ’ is the bulk band gap energy and ‘ E_{exc} ’ is exciton binding energy and ‘ n ’ is the quantum number. Tampo et al. (2007) have reported that the band gap has cubic relation with the oscillator strength and the oscillator strength increases with increase in Mg doping in ZnO. The overlapping and splitting of valence band (VB) and conduction band (CB) states are mainly caused by the Cr impurity band near the Fermi level that has been fused into CB states (Bakhtiar et al. 2014). The widening of band gap in present study results in splitting of VB and CB states due to the blocking of the low-energy transitions by the donor electrons occupying the states at the bottom of the conduction band. This is known as the Burstein–Moss effect (Paul and Venkateswaran 2011). The energy band gap decreases for $x = 0.05$ %, i.e., 3.03 eV. This is because of overlapping of VB and CB states. Hence, Cr dopants act as donors in ZnO and reveal tuning of magnetism in Cr-doped ZnO due to Cr impurities.

The room temperature photoluminescence (PL) spectra of Cr (0, 1, 3 and 5 %)-doped ZnO nanoparticles (Fig. 7)

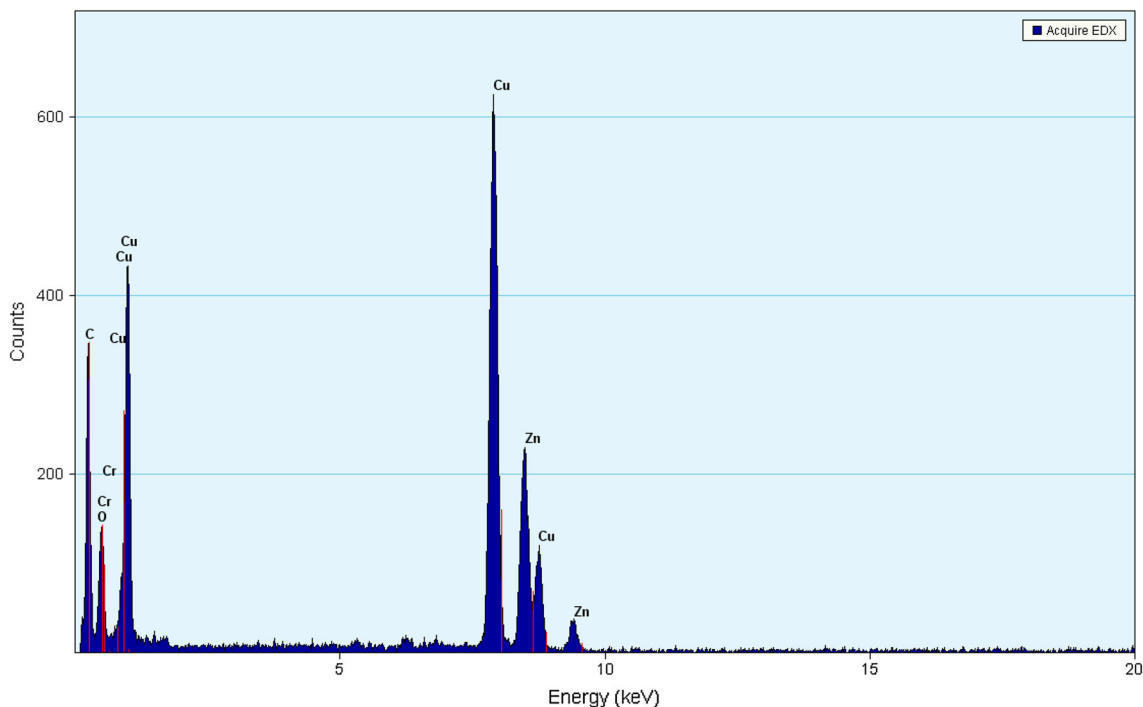


Fig. 4 EDS spectrum of 3 % Cr-doped ZnO nanoparticles

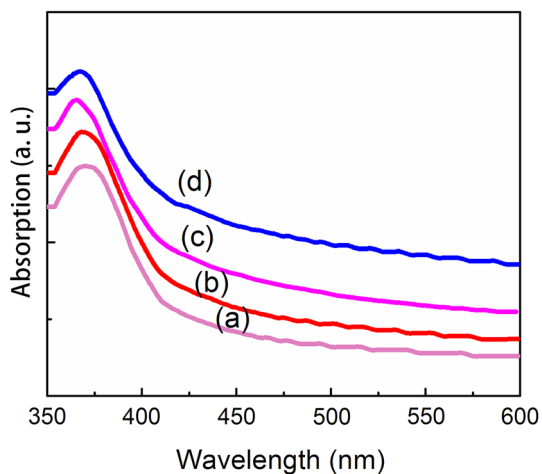


Fig. 5 Optical absorption spectra of $Zn_{1-x}Cr_xO$ (*a–d*) $x = 0, 0.01, 0.03$ and 0.05 , respectively. The position of the peak at 375 nm decreases as x increases

were obtained by utilizing a He–Cd laser of 328 nm wavelength as the excitation source. The violet emission observed around 419 nm is associated to oxygen vacancies (Wang et al. 2006; Kataoka et al. 2010a, b). The violet blue emission peak around 449 nm may be credited to the exciton recombination between the holes in the valence band and electron localized at the interstitial zinc (Karmakar et al. 2007; Kumar et al. 2006). Weak green emission peak observed around 530 nm for 3 and 5 % Cr-doped

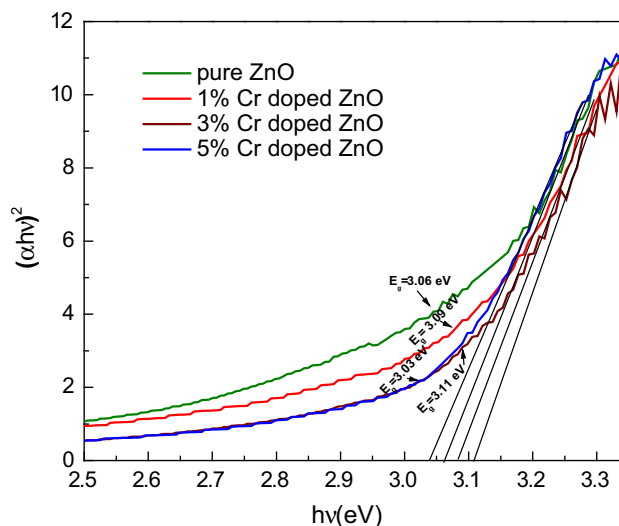


Fig. 6 Tauc's plot of $Zn_{1-x}Cr_xO$ nanoparticles

ZnO, respectively, may be due to the transition between single ionized oxygen vacancy and photoexcited hole, (Vanheusden et al. 1996) or transition between a deeply trapped hole at Vo^{++} (Dijken et al. 2000), surface defects (Djurišić et al. 2004) and electron close to the conduction band. Green emission is usually related with oxygen deficiency while yellow/orange emission is related with excess oxygen (Studenikin et al. 1998). It is observed that the intensity of 485 nm emission increases with increase in Cr

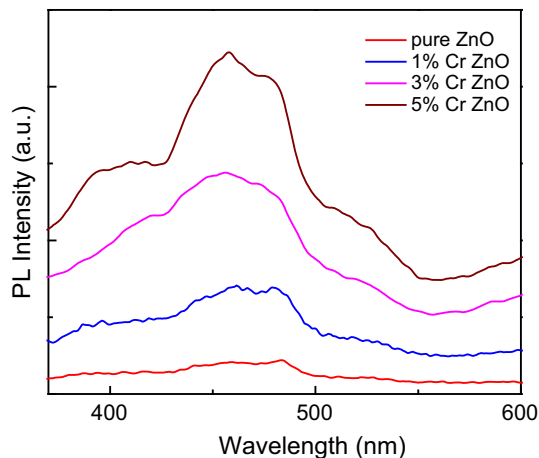


Fig. 7 Room temperature photoluminescence spectra for Cr-doped ZnO nanoparticles

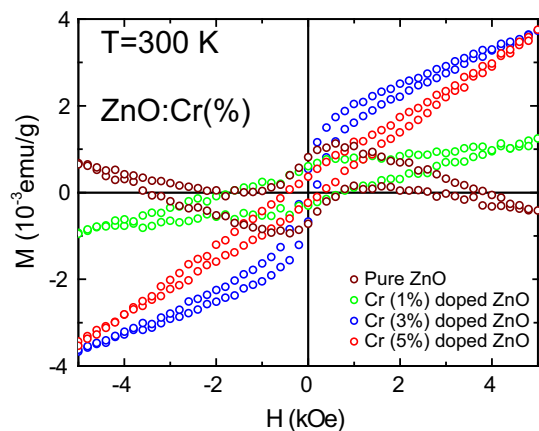


Fig. 8 Room temperature M–H curves for Cr-doped ZnO nanoparticles

content. It is reported that the origin of 485 nm blue emission is due to recombination of bound exciton between a shallow Cr^{3+} donor level and a $V_{\text{Zn}^{2+}}$ acceptor (Chawla et al. 2013).

The magnetic behavior of the as-synthesized $\text{Zn}_{1-x}\text{Cr}_x\text{O}$ nanoparticles is measured at room temperature (300 K) using a magnetic field (H) in the range of -5 kOe to $+5$ kOe as depicted in Fig. 8. Katayama-Yoshida et al. (2007) predicted that Cr is anti-ferromagnetic, the ferromagnetic state in Cr-doped ZnO is more energetically favorable to produce ferromagnetism. The M–H curve for the pure ZnO nanoparticles shows a negative moment with increasing field indicating a diamagnetic behavior of ZnO. Similar results were also reported by Anghel et al. (2010) in ZnO bulk.

In the present study, weak RTFM has been observed for lower concentration of Cr in ZnO. At higher doping concentrations of Cr ($x = 0.05$), there is lack of saturation magnetization even at 5 kOe. It is observed that particle size plays an important role in magnetic properties of the

DMOs. Magnetization increases with decreasing particle size due to the fact that with decreasing particle size, the surface-to-volume ratio increases by increasing the contribution of surface spins to the total magnetic moment of the particle (Park et al. 2007). The band gap values show decrease for $x = 0.05$ of Cr, which means particle size increases for this concentration. With the increase in particle size for $x = 0.05$, magnetization decreases as depicted in Fig. 8. The band gap values of doped ZnO nanocrystals discussed here give a clear insight of finite size effects required for the development of high-density magnetic storage media with nano-sized constituent particles.

The decrease in magnetization at higher concentration is also because of the formation of ZnCr_2O_4 clusters which are anti-ferromagnetic. The secondary peaks corresponding to ZnCr_2O_4 (Cr^{+2}) are depicted in the XRD of Cr-doped ZnO nanoparticles (Fig. 1) correspond to Cr^{+2} . The enhanced anti-ferromagnetic interaction arising from the increased volume fraction of Cr ions suppresses the ferromagnetism in Cr-doped ZnO, which is observed from the decrease in the coercivity observed in these samples. Density of states (DOS) calculations of Mn-doped ZnO by Akai (1998) have revealed a ferromagnetic normal state. This was explained by invoking the double exchange mechanism proposed by Zener (1951) for explaining ferromagnetism observed on doping the anti-ferromagnetic insulator LaMnO_3 . The magnetic behavior in Cr-doped ZnO may arise due to double exchange in case of Cr^{3+} and super-exchange mechanism for Cr^{2+} . In Cr-doped ZnO nanoparticles, the double exchange interaction between free delocalized carriers (hole or electron from the valence band) and the localized d -spins on the Cr ions results in ferromagnetism and super-exchange interactions because of Cr^{+2} ions result in anti-ferromagnetism (Katayama-Yoshida et al. 2007). The observed ferromagnetism is mainly due to the Cr ions substituting for Zn in the ZnO host lattice and not due to Cr metal cluster-like phases. Thus, the injection of Cr into ZnO induces a strong magnetic moment without any distortion in the geometrical symmetry and it also reveals that the ferromagnetic coupling is defined by a double exchange mechanism. Some more experimental studies such as X-ray absorption near-edge structure (XANES) measurements and study of temperature dependence on magnetism are required to relate our observations to the existing theories of ferromagnetism in DMS.

Conclusions

In the present study, $\text{Zn}_{1-x}\text{Cr}_x\text{O}$ nanoparticles have been synthesized successfully through sol–gel technique. Structural analysis indicated that the $\text{Zn}_{1-x}\text{Cr}_x\text{O}$ nanoparticles

were hexagonal in structure with no secondary phase (at low concentrations) indicating that Cr ions are substituted at the Zn sites. Optical absorption studies show that the band gap can be tuned with particle size which is of great importance for device applications. Photoluminescence (PL) studies depict the presence of defects in Cr-doped nanoparticles. The M–H curves at room temperature indicate the presence of weak ferromagnetism. The observed magnetism is explained to be a result of the double exchange in the case of low Cr concentrations and anti-ferromagnetism at higher Cr content due to super-exchange mechanism. These results point to the possibility of tailoring the weak ferromagnetism in ZnO by appropriate Cr doping.

Open Access This article is distributed under the terms of the Creative Commons Attribution License which permits any use, distribution, and reproduction in any medium, provided the original author(s) and the source are credited.

References

- Akai H (1998) Ferromagnetism and its stability in the diluted magnetic semiconductors (In, Mn) As. *Phys Rev Lett* 8:302
- Anghel J, Thurber A, Tenne DA, Hanna CB, Punnoose JA (2010) Correlation between saturation magnetization, bandgap, and lattice volume of transition metal (M = Cr, Mn, Fe Co, or Ni) doped $Zn_{1-x}M_xO$ nanoparticles. *Appl Phys* 107:09E314
- Babu B, Manjari VP, Aswani T, Rao GT, Stella RJ, Ravikumar RVSSN (2014) Structural, optical and magnetic properties of Cr^{3+} doped ZnO Nanopowder. *Ind J Phys* 121:544
- Baibich MN, Brot JM, Fert A, Nguyen Van Dau F, Petroff F (1988) Giant Magnetoresistance of (001)Fe/(001)Cr Magnetic Superlattices. *Phys Rev Lett* 61:2472
- Bakhtiar UH, Ahmed R, Goumri-Said S (2014) Tailoring ferromagnetism in chromium-doped zinc oxide. *Mater Res Exp* 1:016108
- Barnas J, Fuss A, Camley RE, Grunberg P, Zinn W (1990) Novel magnetoresistance effect in layered magnetic structures: theory and experiment. *Phys Rev B* 42:8110
- Chawla S, Sharma S, Kotnala RK (2013) Tailoring magnetic and photoluminescence properties in ZnS/ZnO core/shell nanostructures through Cr doping. *Appl Surf Sci* 284:33
- Dietl T (2002) Ferromagnetic semiconductors. *Semicond Sci Technol* 17:377
- Dijken VA, Meulenkamp EA, Vanmaekelbergh D, Meijerink A (2000) Identification of the transition responsible for the visible emission in ZnO using quantum size effects. *J Lumin* 90:123
- Djurić AB, Choy WCH, Roy VAL, Leung YH, Kwong CY, Cheah KW, Rao TKG, Chan WK, Lui HF, Surya C (2004) Photoluminescence and electron paramagnetic resonance of ZnO Tetrapod Structures. *Adv Funct Mater* 14:856
- Duan LB, Zhao XR, Liu JM, Wang T, Rao GH (2010) Room-temperature ferromagnetism in lightly Cr-doped ZnO nanoparticles. *Appl Phys A* 99:679
- Furdyna JK (1988) Diluted magnetic semiconductors. *J Appl Phys* 64:R29
- Gandhi V, Ganesan R, Syedahamed HHA, Mahalingam T (2014) Effect of cobalt doping on structural, optical and magnetic properties of ZnO nanoparticles synthesized by co-precipitation method. *J Phys Chem C* 188:9715. doi:10.1021/jp411848t
- Karmakar D, Mandal SK, Kadam RM, Paulose PL, Rajarajan AK, Nath TK, Das AK, Dasgupta I, Das GP (2007) Ferromagnetism in Fe-doped ZnO nanocrystals: experiment and theory. *Phys Rev B* 75:144404
- Kataoka T, Kobayashi M, Sakamoto Y, Song GS, Fujimori A, Chang F-H, Lin H-J, Huang DJ, Chen CT, Ohkochi T, Takeda Y, Okane T, Saitoh Y, Yamagami H, Tanaka A, Mandal SK, Nath TK, Karmakar D, Dasgupta I (2010a) Electronic structure and magnetism of the diluted magnetic semiconductor Fe-doped ZnO nanoparticles. *J Appl Phys* 107:3718
- Kataoka T, Yamazaki Y, Sakamoto Y, Fujimori A, Chang FH, Lin HJ, Huang DJ, Chen CT, Tanaka A, Mandal SK, Nath TK, Karmakar D, Dasgupta I (2010b) Electronic structure and magnetism of the diluted magnetic semiconductor Fe-doped ZnO nanoparticles. *Appl Phys Lett* 96:252502
- Katayama-Yoshida H, Sato K (2003) Materials design for semiconductor spintronics by ab initio electronic-structure calculation. *Phys B* 327:337
- Katayama-Yoshida H, Sato K, Fukushima T, Toyoda M, Kizaki H, Dinh VA, Dederichs PH (2007) Theory of ferromagnetic semiconductors. *Phys Stat Sol (a)* 204:15
- Kumar B, Gong H, Vicknesh S, Chua SJ, Tripathy S (2006) Photoluminescence and multiphonon resonant Raman scattering in low-temperature grown ZnO nanostructures. *Appl Phys Lett* 89:071922
- Kumar S, Kaur P, Chen CL, Thangavel R, Dong CL, Ho YK, Lee JF, Chan TS, Chen TK, Mok BH, Rao SM, Wu MK (2014) Structural, optical and magnetic characterization of Ru doped ZnO nanorods. *J Alloys Compd* 588:705
- Li SS, Hu YM (2011) Transition from weak ferromagnetism to strong paramagnetism in $Zn_{1-x}Cr_xO$ ($0 \leq x \leq 0.026$), thin films. *J Phys Conf Ser* 266:012018
- Ohno H (1998) Making nonmagnetic semiconductors ferromagnetic. *Science* 281:951
- Olive-Mendez SF, Santillan-Rodriguez CR, Gonzalez-Valenzuela RA, Espinosa-Magana F, Matutes-Aquino JA (2014) Role of vanadium ions, oxygen vacancies, and interstitial zinc in room temperature ferromagnetism on ZnO-V₂O₅ nanoparticles. *Nanoscale Res Lett* 9:169
- Omria K, Ghoul JE, Lemine OM, Bououdina M, Zhang B, Mir LE (2013) Magnetic and optical properties of manganese doped ZnO nanoparticles synthesized by sol–gel technique. *Superlattice Microstruct* 60:139
- Onodera K, Matsumoto T, Kimura M (1994) 980 nm compact optical isolators using $Cd_{1-x-y}Mn_xHg_yTe$ single crystals for high power pumping laser diodes. *Electron Lett* 30:1994
- Pandiyarajan T, Karthikeyan B (2012) Cr-doping induced structural, phonon and excitonic properties of ZnO nanoparticles. *J Nanopart Res* 14:647
- Park TJ, Papaefthymiou GC, Viescas AJ, Moodenbaugh AR, Wong SS (2007) Size-dependent magnetic properties of single-crystalline multiferroic BiFeO₃ nanoparticles. *Nano Lett* 7(3):766–772
- Paul JD, Venkateswaran C (2011) Bandgap engineering in ZnO by doping with 3d transition metal ions. *J Atom Mol Opt Phys*, Article ID 270540, 7 pages, doi:10.1155/2011/270540
- Pazhanivelu V, Blessington AP, Selvadurai, Murugaraj R (2014) Effect of Ni doping on structural, morphological, optical and magnetic properties of $Zn_{1-x}Ni_xO$ dilute magnetic semiconductors. *J Supercond Nov Magn* 27: 1737
- Sato K, Katayama-Yoshida H (2000) Material design for transparent ferromagnets with ZnO-based magnetic semiconductors. *Jpn J Appl Phys* 39:555
- Sato K, Katayama HY (2002) First principles materials design for semiconductor spintronics. *Semicond Sci Technol* 17:367

- Studenikin SA, Golego N, Cocivera M (1998) Fabrication of green and orange photoluminescent, undoped ZnO films using spray pyrolysis. *J Appl Phys* 84:2287
- Tampo H, Shibata H, Maejima K, Yamada A, Matsubara K, Fons P, Niki S, Tainaka T, Chiba Y, Kanie H (2007) Strong excitonic transition of $Zn_{1-x}Mg_xO$ alloy. *Appl Phys Lett* 91:261907
- Vanheusden K, Seager CH, Warren WL, Tallant DR, Voigt JA (1996) Correlation between photoluminescence and oxygen vacancies in ZnO phosphors. *Appl Phys Lett* 68:403
- Wang H, Wang HB, Yang FJ, Chen Y, Zhang C, Yang CP, Li Q, Wong SP (2006) Structure and magnetic properties of $Zn_{1-x}Co_xO$ single-crystalline nanorods synthesized by a wet chemical method. *Nanotechnology* 17:4312
- Wolf SA, Awschalom DD, Buhrman RA, Daughton JM, Molnar SV, Roukes ML, Chtchelkanova AY, Treger DM (2001) A spin-based electronics vision for the future. *Science* 294:1488
- Zener C (1951) Interaction between the d -Shells in the Transition Metals. II. Ferromagnetic compounds of manganese with perovskite structure. *Phys Rev* 82:403